JGR Solid Earth

RESEARCH ARTICLE
10.1029/2020JB021042

The Viscous and Ohmic Damping of the Earth's Free Core Nutation

Santiago Andrés Triana[1], Antony Trinh[2], Jérémy Rekier[1], Ping Zhu[1], and Véronique Dehant[1]

[1]Reference Systems and Planetology, Royal Observatory of Belgium, Brussels, Belgium, [2]Lunar and Planetary Laboratory, University of Arizona, Tucson, AZ, USA

Key Points:

- We establish asymptotic scaling laws for the free core nutation (FCN)'s Ohmic and viscous dissipation in the fluid core
- Most of the energy dissipation associated with the FCN takes place in the boundary layers
- Our work validates inferences from previous studies that assumed the flow in the outer core as a uniform vorticity flow

Correspondence to:
S. A. Triana,
trianas@oma.be

Citation:
Triana, S. A., Trinh, A., Rekier, J., Zhu, P., & Dehant, V. (2021). The viscous and Ohmic damping of the Earth's free core nutation. *Journal of Geophysical Research: Solid Earth*, *126*, e2020JB021042. https://doi.org/10.1029/2020JB021042

Received 24 SEP 2020
Accepted 4 MAR 2021

Abstract The cause for the damping of the Earth's free core nutation (FCN) and the free inner core nutation eigenmodes has been a matter of debate since the earliest reliable estimations from nutation observations were made available. Numerical studies are difficult given the extreme values of some of the parameters associated with the Earth's fluid outer core, where important energy dissipation mechanisms can take place. We present a fully 3D numerical model for the FCN capable of describing accurately viscous and Ohmic dissipation processes taking place in the bulk of the fluid core as well as in the boundary layers. We find an asymptotic regime, appropriate for Earth's parameters, where viscous and Ohmic processes contribute to the total damping, with the dissipation taking place almost exclusively in the boundary layers. By matching the observed nutational damping, we infer an enhanced effective viscosity matching and validating methods from previous studies. We suggest that turbulence caused by the Earth's precession can be a source for the enhanced viscosity.

Plain Language Summary Gravitational pull from the Sun and the moon (tidal forces) cause small periodic changes in the orientation of the Earth's spin axis, which can be measured very precisely by using radiotelescope observations of very distant quasars around the sky. It turns out that there is a small time delay between the tidal force and the Earth's spin axis response indicating that there is some process inside the Earth that is dissipating energy. Here we perform a numerical simulation to see if there is energy being lost inside the fluid outer core of the Earth. We find that there is minimal energy lost in the bulk of the core and that most of the energy is being lost at the interface between the fluid core and the Earth's mantle. Previous studies have assumed without proper justification that energy dissipates only at the fluid-solid interface. Thus our study validates such assumption.

1. Introduction

The orientation of Earth's rotation axis is continuously changing in time as a response to the tidal forces exerted by the Moon, the Sun, and the planets. As seen from an inertial frame, the time scales involved in these changes range from thousands of years, as in the case of precession, to months and days in the case of nutations. The tidal forcing in the diurnal frequency range (as seen from a frame attached rigidly to the mantle) causes the resonant excitation of two eigenmodes, the free core nutation (FCN) and the free inner core nutation (FICN). These modes can be pictured as solid-body rotations of the fluid outer core and the solid inner core, respectively, along axes slightly different than that of the mantle. Commonly referred to as *rotational* eigenmodes, they are in fact coupled to the *inertial* eigenmodes of a rotating fluid (Rekier et al., 2020; Triana et al., 2019). An important example of the latter is the *spin-over* eigenmode, which is mostly a uniform-vorticity flow in a *uniformly rotating* rigid boundary (Greenspan, 1968). Instead, if we allow the boundaries to exchange angular momentum with the fluid core, we obtain the familiar FCN eigenmode. The real part of the associated eigenvalue corresponds to the damping decay factor, while the imaginary part corresponds to the frequency (a real number). Alternatively, the damping decay factor (or simply "the damping") can be represented as the imaginary part of the frequency, now a complex number. Here, we focus on the damping of the FCN, which corresponds mainly to the imaginary part of the coupling constant K_{CMB} introduced by Mathews et al. (2002), see also Equation 16b in Koot et al. (2010).

The tidal forcing on the Earth and its spin axis orientation response are known very precisely. The observed phase lag between the tidal forcing and Earth's response, particularly the annual retrograde nutation, helps

us infer the total power dissipated in the Earth's interior (Mathews et al., 2002). In other words, the observed nutations allow us to determine $\mathrm{Im}\{K_{\mathrm{CMB}}\}$, of which the latest estimate is $(-1.78 \pm 0,02) \times 10^{-5}$ (Koot et al., 2010). The damping in the fluid core is viscous and Ohmic in nature given the magneto-hydrodynamic character of the flow, and modeling such flow is difficult not only because of the fluid core's very low Ekman number $E \sim 10^{-15}$ (i.e., the ratio of viscous to Coriolis forces, see Section 2.2) but also because the geomagnetic field there is largely unknown.

Downward continuation of the observed magnetic field at the Earth's surface offers a glimpse of the large-scale magnetic field (i.e., associated with spherical harmonic degrees $\ell \leq 13$) at the core-mantle boundary (CMB). The inferred *rms* value of the radial component of the dipolar field at the CMB, denoted B_r^{D}, is about 0.21 mT. The *rms* value of the remaining non-dipolar components, B_r^{ND}, is estimated to be around 0.28 mT. This, however, is an estimate based on the spectral trend of the observed, large-scale field up to $\ell = 13$, which might not be representative of the actual small-scale field. Unfortunately, the strong magnetization of the Earth's crust prevents a reliable characterization of the small-scale field for $\ell > 13$.

By assuming a thin and electrically conducting layer with a conductivity of 5×10^5 S/m at the bottom of the mantle, Buffett (1992) could explain the anomalous out-of-phase amplitude of the annual retrograde nutation, although he noted that purely viscous dissipation at the CMB, with a kinematic viscosity $\nu = 0.1$ m^2 s^{-1} could explain the anomaly alternatively. Later Buffett et al. (2002) showed that the damping inferred from nutations could be explained by an overall *rms* radial magnetic field at the CMB of about 0.69 mT, with a non-dipolar part taking up 0.64 mT, appreciably larger than the inferred 0.28 mT mentioned above. The study considers the Ohmic heating losses in both the fluid and in the thin conductive layer but assumes no viscosity, that is, the coupling torque is purely electromagnetic. Alternatively, Palmer and Smylie (2005) assumed a purely viscous coupling torque and estimated an Ekman number of $E \sim 9 \times 10^{-11}$ to match the inferred damping from nutations. This estimate is about five orders of magnitude larger than the expected Ekman number based on the molecular viscosity of the fluid core (Gans, 1972). Viscous and electromagnetic coupling torques on the mantle can be both taken into account simultaneously, but their relative contribution cannot be disentangled easily. The key quantities are the conductivity of the hypothetical thin conductive layer at the bottom of the mantle, often assumed to match the conductivity of the fluid core, and the strength of the non-dipolar part B_r^{ND} of the magnetic field at the CMB. Mathews and Guo (2005) assumed a B_r^{ND} ranging from 0.252 to 0.645 mT and three different values of the conductivity (5×10^5 S/m matching the fluid core, 5×10^4 S/m, and 10 S/m) for the bottom layer of the mantle. They concluded that inferred $\mathrm{Im}\{K_{\mathrm{CMB}}\}$ requires the presence of some viscous dissipation in the fluid core except in the high conductivity, high B_r^{ND} case as already noted by Buffett (1992) and Buffett et al. (2002).

A more detailed treatment of the magnetic field power spectrum was carried out by Deleplace and Cardin (2006). They truncated their magnetic models at $\ell_{\max} = 40$ and noted that the non-dipolar component of the field is not strong enough to warrant a purely electromagnetic coupling, even if the thin layer at the bottom of the mantle had the same conductivity as the fluid core. They propose an Ekman number of the order of 10^{-11} to compensate for the reduced electromagnetic torque. The study by Buffett and Christensen (2007) extends the truncation level to $\ell_{\max} = 160$ or higher in their proposed magnetic field. They argue that such a field, although not supported by the observed magnetic spectrum at the Earth's surface, is strong enough to provide an *rms* value of 0.66 mT to the non-dipolar component while still being physically plausible given the geodynamo's tight energy budget (Christensen & Aubert, 2006). The studies from Buffett and Christensen (2007) and Koot et al. (2010) dismiss the contribution of viscous dissipation to the coupling constant because the required viscosity, interpreted as an effective eddy viscosity by Deleplace and Cardin (2006), would involve turbulent eddies with typical sizes and turnover times largely incompatible with the boundary flow associated with nutations. The study by Koot and Dumberry (2013) determined that the particular morphology of the non-dipolar part of the field is largely unimportant when it comes to the torque estimation, what matters most is simply its effective *rms* value at the CMB.

Common to most of the works mentioned so far is the assumption that the core flow is simply a solid body rotation with a correction required only near the boundaries, disregarding dissipation processes that might take place in the bulk of the fluid. This assumption does not necessarily always hold because other eigenmodes might interact with uniform vorticity flows as demonstrated by Triana et al. (2019) (see also Rogister & Valette (2009) and Schmitt (2006)). The resulting flow in the interior can thus deviate considerably from

solid body rotation. There is also the possibility of internal shear layers spawned by eruptions from the Ekman boundary layers at the critical latitudes (Rieutord et al., 2001). Such internal shear layers are the seat of appreciable amounts of viscous and Ohmic dissipation, which is sometimes dominant (Buffett, 2010; Lin & Ogilvie, 2018). Thus, to investigate possible dissipation processes in the bulk of the core and assess the validity of the solid body rotation approximation, we investigate numerically a linear 3D model of the FCN's damping by studying its closely related and purely inertial counterpart, the spin-over mode (Rekier et al., 2020). We represent the Earth's geomagnetic field as an imposed magnetic field either as an axial uniform or as a dipolar field. We assume an insulating mantle and inner core, thus drawing our conclusions for the case of no electromagnetic torque. A more detailed description of the model follows.

2. A Model for the Free Core Nutation

2.1. General Assumptions

The Earth's FCN is essentially a global eigenmode in which the mantle's spin axis does not coincide with the fluid core spin axis. Although both axes experience a small and periodic oscillation in their orientation as seen from an inertial frame, their relative orientation angle remains constant. The FCN frequency is nearly diurnal as seen from a reference frame attached rigidly to the mantle. During the FCN motion, the kinetic energy associated with the oscillation of the spin axis of the fluid core is much larger than the respective oscillation of the mantle.

A few simplifications are possible leading to a numerically tractable model for the FCN's energy dissipation. First, given that most of the FCN's energy is carried by the fluid core, we assume the mantle to be rigid and uniformly rotating, ignoring elastic deformations and small deviations from uniform rotation. Doing so allows us to represent the FCN as the spin-over mode introduced earlier. Second, since most of the energy dissipation takes place in the boundary layers and depends only weakly on small deviations of the boundaries from sphericity (see Appendix B), we model both the ICB and the CMB as spherical surfaces. Additionally, we assume an incompressible fluid core with uniform electrical conductivity σ and density ρ, together with no-slip boundary conditions for the flow velocity, and electrically insulating mantle and inner core. We chose insulating boundaries because of their computational convenience, allowing us at the same time to focus on dissipative processes exclusively within the fluid core. To represent the geomagnetic field we adopt a static, imposed magnetic field of the form $\boldsymbol{B}_0 = -\nabla\Phi$ where Φ is a scalar function expanded in the spherical harmonics basis as

$$\Phi(r,\theta,\phi) = \sum_{l,m} h_{lm}(r) Y_l^m(\theta,\phi). \tag{1}$$

We consider two simple axisymmetric ($m = 0$) morphologies with $l = 1$: an axial uniform field with $h_{10}(r) = -B_0\, r$, and a dipolar field with $h_{10}(r) = B_0/(2r^2)$ both aligned with the mantle's rotation axis $\hat{\mathbf{z}}$. The *rms* value of the radial magnetic field at the CMB is in both cases $B_0 / \sqrt{3}$. Figure 1 shows a schematic of the two configurations.

2.2. Governing Equations

We compute the eigenmodes of our system as follows. We use the CMB radius R as the unit of length, the inverse angular speed of the Earth Ω^{-1} as the unit of time (or rotation time scale), and B_0 as the unit for the magnetic field strength. Then, in a reference frame attached rigidly to the mantle, small deviations of the flow velocity $\boldsymbol{u}$ and magnetic field $\boldsymbol{b}$ from their steady state obey the linearized Navier-Stokes and induction equations

$$\begin{aligned} \frac{\partial \mathbf{u}}{\partial t} + 2\hat{\mathbf{z}} \times \mathbf{u} &= -\nabla p + E\nabla^2 \mathbf{u} + Le^2 (\nabla \times \mathbf{b}) \times \mathbf{B_0}, \\ \frac{\partial \mathbf{b}}{\partial t} &= \nabla \times (\mathbf{u} \times \mathbf{B_0}) + E_\eta \nabla^2 \mathbf{b}, \end{aligned} \tag{2}$$

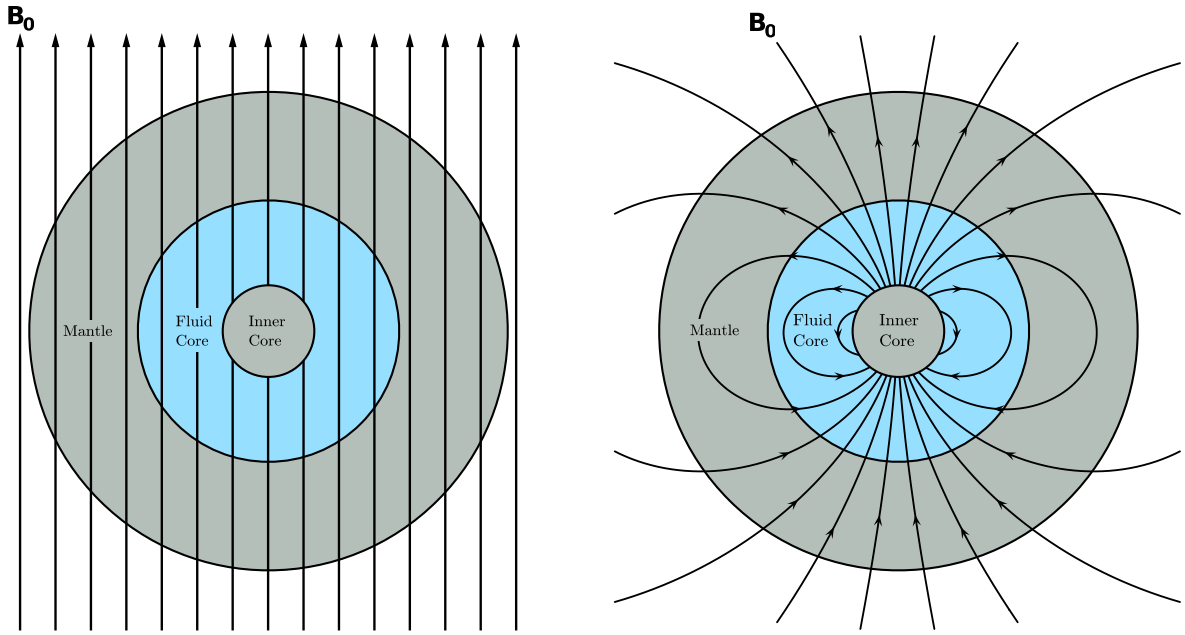

Figure 1. Schematic view of our Earth model with an imposed magnetic field $\boldsymbol{B_0}$, which we consider as axial uniform (left) or dipolar (right). The ratio between the solid inner core radius and the fluid outer core radius is 0.35.

where p is the (dimensionless) reduced pressure. The Ekman number E is the ratio between the rotation time scale Ω^{-1} and the viscous diffusion time scale R^2/ν, the Lehnert number Le is the ratio between the Alfvén speed $B_0 \,/\, \sqrt{\rho\mu_0}$ and the unit of speed ΩR, and the magnetic Ekman number E_η is the ratio between the rotation time scale and the magnetic diffusion time scale R^2/η:

$$E = \frac{\nu}{\Omega R^2}, \quad Le = \frac{B_0}{\sqrt{\rho\mu_0}\,\Omega R}, \quad E_\eta = \frac{\eta}{\Omega R^2}, \tag{3}$$

where ν is the kinematic viscosity (or momentum diffusivity), η is the magnetic diffusivity, and μ_0 is the magnetic permeability. We complement Equation 2 with no-slip boundary conditions for $\mathbf{u}$ and insulating boundary conditions for $\boldsymbol{b}$. Alternatively to Le and E_η, the Elsasser number Λ representing the ratio of Lorentz to Coriolis forces and the magnetic Prandtl number P_m representing the ratio of viscosity to magnetic diffusivity can also be used as control parameters. They can be written as

$$\Lambda = \frac{Le^2}{E_\eta}, \quad P_m = \frac{E}{E_\eta}. \tag{4}$$

The parameters Λ and P_m turn out to be better suited when searching for scaling laws appropriate for Earth (see Sections 3 and 4). We seek for eigenmodes as solutions of Equation 2, so we write $\boldsymbol{u}$ and $\boldsymbol{b}$ as

$$\mathbf{u}\big(\mathbf{r},t\big) = \mathbf{u}_0(\mathbf{r})\mathrm{e}^{\lambda t} + \mathrm{cc}, \quad \mathbf{b}(\mathbf{r},t) = \mathbf{b}_0(\mathbf{r})\mathrm{e}^{\lambda t} + \mathrm{cc}, \tag{5}$$

where $\lambda = \sigma + \mathrm{i}\omega$ is a complex number whose real part σ corresponds to the damping factor and the imaginary part ω to the eigenfrequency. We add the complex conjugate (cc) to keep $\boldsymbol{u}$ and $\boldsymbol{b}$ real. The details about the discretization scheme that we use to cast problem Equation 2 as a generalized eigenvalue problem, and the numerical method to solve it, can be found in Appendix A, see also Rekier et al. (2019). Solving the eigenvalue problem provides us with several inertial eigenmodes as solutions, from which the spin-over mode needs to be identified. This is easily accomplished since the spin-over mode, being characteristically an

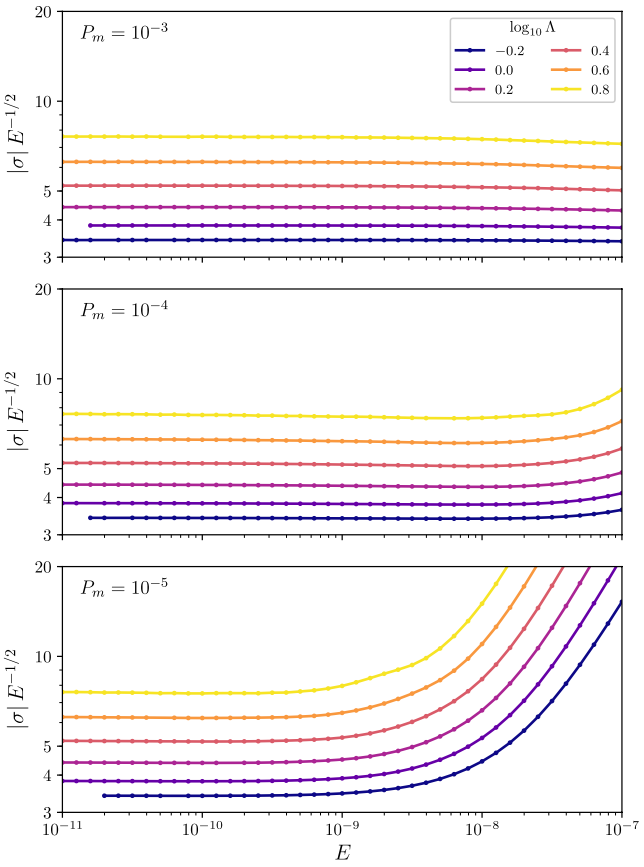

Figure 2. The Ekman number at which the asymptotic regime is reached depends on Λ and P_m. Here we show the scaled damping $|\sigma|E^{-1/2}$ versus E for three different values of P_m. Color indicates $\log_{10}\Lambda$. Here the imposed magnetic field is axial and uniform.

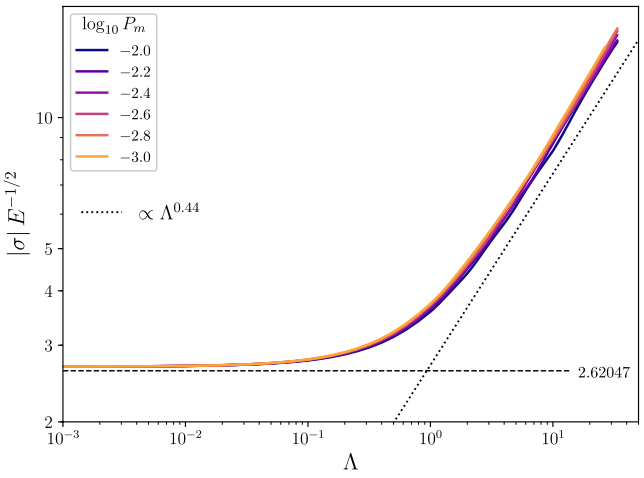

Figure 3. The asymptotic value of $|\sigma|E^{-1/2}$ computed at $E = 10^{-9}$ for $10^{-3} \le P_m \le 10^{-2}$ and $10^{-3} \le \Lambda \lesssim 30$, imposed axial uniform field case. The dashed horizontal line indicates the theoretical asymptotic value (≈2.62047) in the no inner core, purely hydrodynamic case. The dotted line represents a $\Lambda^{0.44}$ scaling law for reference.

almost uniform vorticity flow, is the only one with a toroidal component much larger than its poloidal component.

We have thus three control parameters: E, Λ, and P_m, which in principle we can vary at will, except for the Ekman number. The small length scale features associated with the very small E for the Earth's core ($E \sim 10^{-15}$ if we use the molecular value for the viscosity, $\nu \sim 10^{-6}$ m^2 s^{-1}) are out of reach numerically. We study our problem by considering the lowest E as computationally feasible (down to $E \sim 10^{-11}$ for the axial uniform field and $E \sim 10^{-9}$ for a dipolar field, a limitation due mainly to high memory usage and round-off errors) and see if we approach any kind of asymptotic behavior.

3. Imposed Axial Uniform Magnetic Field Case

For illustrative purposes we start by setting the Elsasser number Λ with a value between $10^{-0.2} \approx 0.63$ and $10^{0.8} \approx 6.3$, and three different values for P_m. For comparison, Earth's values are $P_m \approx 10^{-6}$, and $\Lambda \approx 1$ if we take a *total* rms radial magnetic field at the CMB of 0.7 mT. Note that we define the Elsasser number in Equation 4 based on the strength B_0 of the uniform background magnetic field which has an *rms* radial magnetic field average $B_r^{\rm rms} = B_0 / \sqrt{3}$. The results for the damping σ of the spin-over mode are shown in Figure 2. An asymptotic behavior is reached at low values of E, depending on Λ and P_m. When $P_m = 10^{-3}$ our results show that $\sigma \propto E^{1/2}$ for practically all chosen values of Λ (top panel, Figure 2). At $P_m = 10^{-4}$ (center panel) the asymptotic regime is reached when $E \lesssim 10^{-8}$ for $\Lambda \approx 6.3$, or when $E \lesssim 10^{-7.6}$ for $\Lambda \approx 0.63$. Decreasing P_m further to 10^{-5} (bottom panel) pushes the beginning of the asymptotic regime down to $E \lesssim 10^{-9.5}$ for $\Lambda \approx 6.3$, and to $E \lesssim 10^{-9}$ when $\Lambda \approx 0.63$. The value of $|\sigma|E^{-1/2}$ in the asymptotic regime increases with increasing Λ from the purely hydrodynamic value of 2.62047 (see Appendix B) to about 8 for $\Lambda \approx 6.3$. In the asymptotic regime, $\sigma E^{-1/2}$ depends only weakly on P_m.

In Figure 3, we show the asymptotic value of $|\sigma|E^{-1/2}$ (computed at $E = 10^{-9}$) as a function of both Λ and P_m. When $\Lambda \ll 1$ we are essentially in the purely hydrodynamic regime and $|\sigma|E^{-1/2}$ is very close to the hydrodynamic value, independent of Λ and P_m. A clearly distinct regime appears when $\Lambda \gtrsim 5$. In this regime the damping σ behaves approximately as

$$\sigma(P_m, \Lambda, E) = -c(P_m)\Lambda^{\alpha(P_m)}E^{1/2}, \tag{6}$$

where c and α depend only weakly on P_m, see Figure 4. We could not explore the asymptotic regime at even higher Λ since it would require calculations with Ekman numbers smaller than our current numerical limit of 10^{-11}.

The asymptotic damping is almost entirely viscous when $\Lambda \ll 1$, with the ratio $\mathcal{D}_\eta / \mathcal{D}_\nu \propto \Lambda$. In this "weak field" regime the damping is practically independent of P_m (as long as P_m is much smaller than unity), and it seems to follow

$$\sigma(\Lambda, E) = -\Big(2.676 + 1.10\Lambda\Big)E^{1/2}, \tag{7}$$

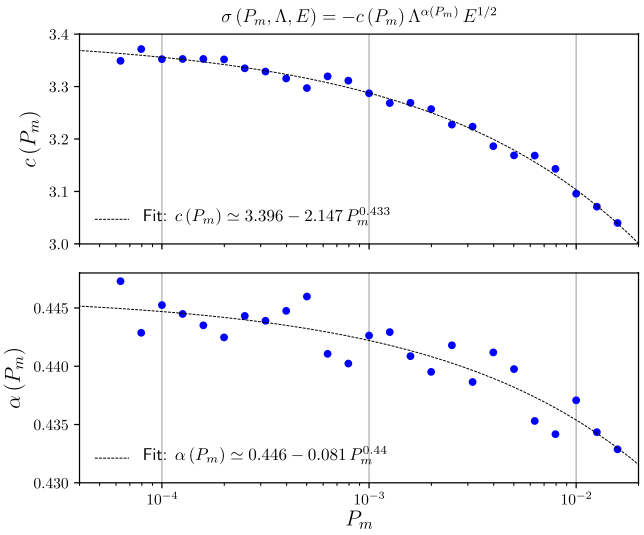

Figure 4. Dependence of the fit parameters c (top) and α (bottom) describing the asymptotic damping of the spin-over mode when $\Lambda \gtrsim 5$, see Equation 6. Imposed axial uniform field case.

which comes from a fit from solutions computed at $E \leq 10^{-9}$. At $\Lambda = 0$ the expression above gives $\sigma\, E^{-1/2} = -2.676$ which is reasonably close to the theoretical value -2.62047 computed for a *full* sphere (Greenspan, 1968; Zhang et al., 2004). When $\Lambda \gtrsim 1$ Ohmic and viscous dissipation contribute nearly equally to the total damping, independently of Λ, see Figure 5.

To conclude this section, we show that the imaginary part of the coupling constant, $\mathrm{Im}\{K_{\mathrm{cmb}}\}$, is related in a simple way to the damping σ, both providing essentially the same information. Let us assume that the core flow can be represented approximately as a solid body rotation around an equatorial axis with angular speed $\Omega_f(t)$. It suffices for our purpose to consider just the magnitude Ω_f. The damping σ would represent the inverse time constant associated with the free decay of that motion. The magnitude γ of the viscous torque is simply $\gamma = \mid I\dot{\Omega}_f \mid = I \mid \sigma \mid \Omega_f \mid$ where I is the moment of inertia of the fluid core. According to our non-dimensionalization scheme, and with the fluid density set as unity we write

$$I = \frac{8\pi}{15}\left(1 - R_{\mathrm{icb}}^5\right). \tag{8}$$

The amplitude of the eigenmode solution provided by our matrix solver is such that its total kinetic energy is set to unity, thus $\Omega_f = \sqrt{2\,/\,I}$. So, in our dimensionless variables we have

$$\frac{\gamma}{\sqrt{2I}} = \mid \sigma \mid, \quad \tilde{\gamma} \equiv \frac{\gamma}{\mid \sigma \mid \sqrt{2I}}. \tag{9}$$

Note that the damping is a global quantity, and thus it is related to the total torque on the core, including that at the inner-core boundary. However, in the asymptotic regime, the torque on the CMB alone accounts for more than 98% of the damping, see Figure 6. Then the coupling constant $\mathrm{Im}\{K_{\mathrm{cmb}}\}$ can be read directly from the damping σ, overestimating it only by less than 2%.

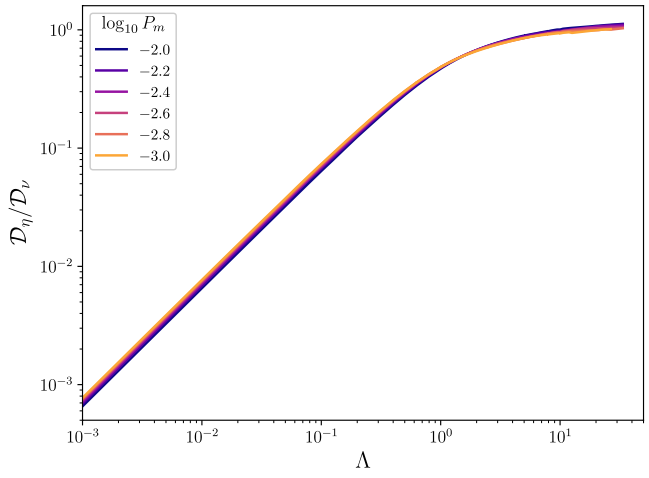

Figure 5. The ratio of Ohmic to viscous dissipation $\mathcal{D}_\eta\ /\ \mathcal{D}_\nu$ computed at $E = 10^{-9}$. Imposed axial uniform field case.

4. Imposed Dipolar Field Case

We proceed in a similar way as in the axial uniform magnetic field case, trying to reach the smallest E as possible for different combinations of Λ and P_m. It turns out that poor numerical convergence and round-off errors manifested already in the dipolar case at around $E \sim 10^{-8}$ for some values of Λ and P_m, and a twice as high truncation level compared to the uniform field case (both in radial and angular direction) was generally required to obtain satisfactory solutions. Notwithstanding, we could get a glimpse of the asymptotic regime for the geophysically relevant case of $\Lambda \sim 0.1$, which corresponds to the estimated radial rms strength of 0.21 mT of the *dipolar* component of the magnetic field at the CMB. Figure 7 shows the scaled damping at $\Lambda = 0.1$ for a range of P_m as a function of E. The asymptotic regime appears below $E \sim 10^{-6}$ for $P_m = 0.1$, while it seems to appear below $E \sim 10^{-9}$ for $P_m = 10^{-4}$. As in the axial uniform field case, the asymptotic scaled damping appears to be weakly dependent on P_m, at least for $\Lambda = 0.1$.

We turn now to the Λ-dependence of the damping in the asymptotic regime. Figure 8 shows how the asymptotic value of $|\sigma|E^{-1/2}$ depends on the Elsasser number Λ, for a few values of P_m. Due to the numerical difficulties mentioned above, we could only cover relatively small ranges of Λ for each P_m. The constant $c = 2.678986$ as used in the figure is chosen

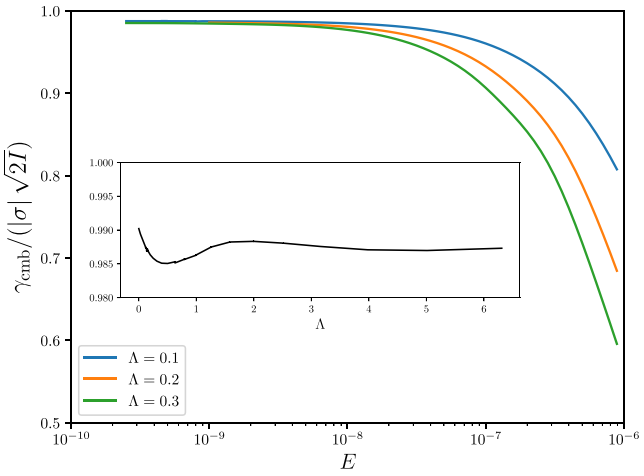

Figure 6. The ratio $\tilde{\gamma}$ between the computed CMB viscous coupling torque $\gamma_{\rm cmb}$ / $\sqrt{2I}$, and the mode damping σ. The ratio $\tilde{\gamma}$ should approach unity if the flow is mostly a solid body rotation whose damping is due solely to torques on the outer boundary. In the main figure, we fix $P_m = 10^{-4}$. The inset plot, where we fix $E = 10^{-9}$ and $P_m = 10^{-3}$, shows little variation of the ratio $\tilde{\gamma}$ over an extended range of Λ. Imposed axial uniform field case. CMB, core-mantle boundary.

after a fit of of the form $\sigma = -(c + k\,\Lambda^{\alpha})E^{1/2}$ using only the solutions with $P_m = 10^{-4}$. The plot suggests that c, k, and α indeed depend on P_m for $\Lambda \lesssim 3 \times 10^{-3}$ but become only weakly dependent on P_m for $\Lambda \gtrsim 3 \times 10^{-3}$. The exponent in Λ^{α} is very close to 1 for $P_m = 10^{-4}$ and $\Lambda < 3 \times 10^{-3}$, while becoming very close to 2/3 for higher Λ. So, for $\Lambda > 3 \times 10^{-3}$ the damping is approximately

$$\sigma \approx -\left(2.679 + 1.74\Lambda^{2/3}\right)E^{1/2}, \tag{10}$$

as long as $P_m \ll 1$. We discuss the CMB torque and the Ohmic to viscous dissipation ratio further below in Section 5.

5. Discussion

5.1. Boundary Layer Scaling

The damping of the spin-over mode with an axial uniform magnetic field background follows a familiar $E^{1/2}$ asymptotic scaling even for moderate values of the Elsasser number Λ above 1. This scaling is intimately connected to the fact that most of the energy dissipation, whether Ohmic or viscous, takes place at the boundary layers. The character of the boundary layers transitions from an Ekman layer type when $\Lambda \ll 1$ to a slightly thinner Hartmann-Ekman layer type when $\Lambda \sim \mathcal{O}(1)$, in accordance with Benton and Loper (1969). Figure 9 shows the radial (θ, ϕ integrated) profiles of the viscous and Ohmic dissipation near the CMB for both cases, which clearly demonstrate the *thinner* boundary layer for a larger Elsasser number. The different curves collapse onto one when scaling the radial distance to the CMB by $E^{1/2}$ matching the asymptotic scaling of the damping. The damping in the imposed dipolar field case exhibits the same scaling, thus suggesting the same scaling for the width of the boundary layers, but we could not verify this directly given the rather narrow range of Ekman numbers that we could study in the asymptotic regime in that case.

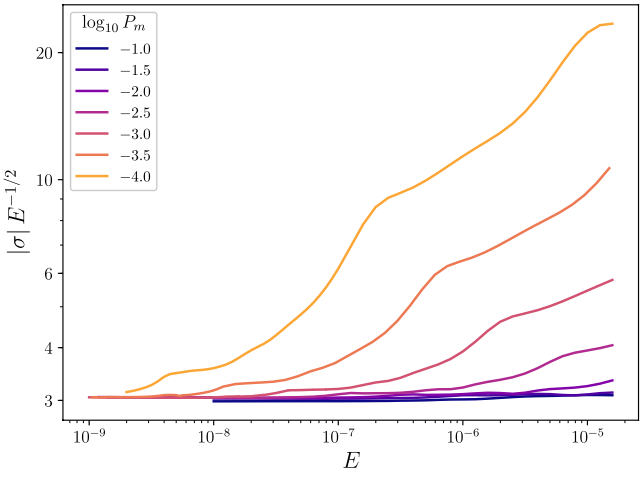

Figure 7. In the imposed dipolar field case, the asymptotic regime for the damping appears at values of E depending on P_m, in a similar fashion as in the axial uniform field case. However, numerical convergence of the solutions is much harder to achieve compared to axial uniform field case; therefore, we could only explore here a limited range of the control parameters. In this plot, the Elsasser number is fixed at $\Lambda = 0.1$.

5.2. Axial Uniform Versus Dipolar Field Background

The behavior of the spin-over mode for an extended range of Ekman numbers in the dipolar background field case is qualitatively similar to the axial uniform case. Figure 10 illustrates this point. The main difference being an overall increase in the total damping in the dipolar case. In both cases, there is a damping peak near $E \sim 10^{-5}$ for $P_m = 10^{-4}$ and near $E \sim 10^{-4}$ for $P_m = 10^{-3}$ (i.e., when $E_\eta \sim 0.1$) appearing also as a peak in the mode frequency (top right panel), as a valley in the CMB torque to dissipation ratio $\tilde{\gamma}_{\rm cmb}$ (bottom left panel), and again as a peak in the total Ohmic to viscous dissipation ratio (bottom right panel). The marked departure from unity of the ratio $\tilde{\gamma}$ is indicative of considerable energy dissipation taking place in the *bulk* of the fluid compared to the boundaries at larger E. In this situation, the damping σ is therefore *not* expected to scale as $E^{1/2}$ as it is not the case indeed away from the asymptotic range. The spin-over mode is still unambiguously identifiable as the mode with the largest toroidal to poloidal kinetic energy ratio, but the induced magnetic field seems weakly coupled to the flow. This peculiar behavior near $E_\eta \sim 0.1$ is very reminiscent of magnetic free decay modes where the magnetic field dynamics is dominated by magnetic diffusion (see e.g., Moffatt & Dormy, 2019; Schmitt, 2012); however, we did not investigate this in further detail since it seems beyond the scope of our geophysical setting.

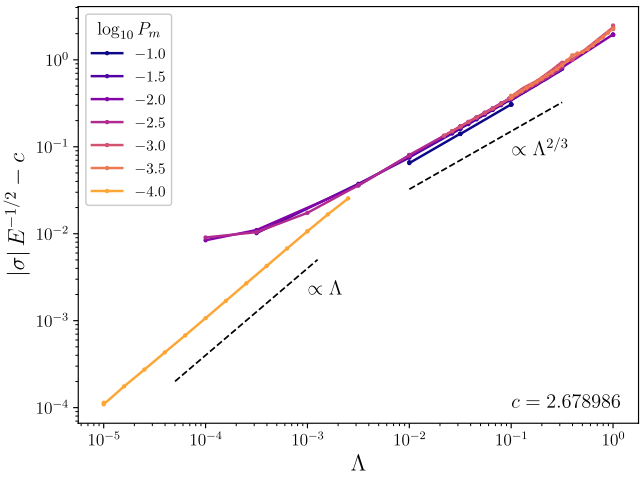

Figure 8. A plot of $|\sigma|E^{-1/2} - c$ with $c = 2.678986$ as a function of Λ for a range of P_m in the imposed dipolar field case. The asymptotic value of $|\sigma|E^{-1/2}$ appears to depend on P_m for $\Lambda \ll 1$, as opposed to the axial uniform case. A regime transition takes place near $\Lambda = 3 \times 10^{-3}$. At $\Lambda = 0.1$, corresponding roughly to the radial rms strength of the dipolar component of Earth's magnetic field at the CMB, the asymptotic value seems independent of P_m, especially for $P_m \ll 1$. CMB, core-mantle boundary.

It is clear from the top right panel of Figure 10 that for fixed Λ and P_m the asymptotic regime appears at much lower Ekman numbers in the dipole case, and the asymptotic value of the scaled damping is slightly higher. The ratio $\tilde{\gamma}$ (see Equation 9) for the CMB in the asymptotic regime is not as close to unity in the dipolar case as in the axial uniform case. This is not surprising since the background magnetic field is stronger near the ICB in the dipolar case; thus, we expect a larger contribution to the total damping from the dissipation at the ICB, coming from comparatively more Ohmic dissipation, and correspondingly higher ICB torque. In both cases, the frequency of the spin-over mode in the *asymptotic* regime becomes very close to one, as can be seen from the top right panel in Figure 10. The frequency dependence of this mode, or the Earth's FCN for that matter, is dominated mainly by the flattening of the planet, which our study ignores.

5.3. Comparing to Observations

We now compare the damping of the spin-over mode with values deduced from Earth's annual retrograde nutation observations, that is, with the imaginary part of the CMB coupling constant which Koot et al. (2010) report as $\mathrm{Im}\{K_{\mathrm{CMB}}\} = (-1.78 \pm 0.02) \times 10^{-5} \equiv \sigma_{\mathrm{obs}}$. Let us assume now that either Equation 6 or Equation 10 correctly describe Earth's core regime and extrapolate toward the appropriate Ekman number, $E = 10^{-15}$, which is based on a molecular kinematic viscosity of $\nu \approx 10^{-6}$ m^2 s^{-1}. Equation 6 then shows that Λ needs to be quite large ($\Lambda \approx 10^5$) at $E = 10^{-15}$ to match σ_{obs}. This would correspond to a radial *rms* magnetic field of about 220 mT at the CMB. In the dipolar background field case, Equation 10 requires a somewhat smaller radial *rms* field of about 120 mT at the CMB to match σ_{obs}, which is still incompatible with the downward continuation of the observed magnetic field at the Earth's surface. Alternatively, if we require $\Lambda \sim \mathcal{O}(1)$ then the Ekman number must be $E \sim \mathcal{O}(10^{-11})$. Such a high Ekman number might arise as the result of turbulent behavior in the boundary layers, in which case the *effective* kinematic viscosity is better represented by an *eddy* viscosity $\nu_e \sim 2.2 \times 10^{-2}$ m^2 s^{-1} rather than its molecular value. Note however that our choice of an insulating mantle might not be realistic and another interpretation is possible. As we discussed in the introduction, the damping could be explained as well by a purely electromagnetic coupling through a hypothetical thin layer of electrically conductive material at the bottom of the mantle.

It is certainly the case that the FCN flow velocity at the CMB associated with the retrograde annual nutation is not large enough to drive instabilities leading to turbulence. With roughly 32 mas of observed amplitude, it leads to a core surface velocity of only 1.7×10^{-4} m/s. The corresponding Reynolds number, defined as $Re = v\delta/\nu$, where $\delta = R_{\mathrm{cmb}}\sqrt{E}$ is the width of the boundary layer, v the core surface velocity and ν the kinematic viscosity, is $Re = 21$. The boundary flow is known to become unstable only at $Re \sim 55$ and fully turbulent at $Re \sim 150$ (Cébron et al., 2019; Lorenzani & Tilgner, 2001; Sous et al., 2013). On the other hand, Earth's precession is very likely to drive a turbulent boundary flow at the CMB. This precessional motion leads to an angular misalignment between the fluid core spin axis and the instantaneous mantle spin axis. According to Tilgner (2007) and Le Bars et al. (2015) the misalignment is 1.7×10^{-5} radians, an estimate based on the theory by Busse (1968) for a fluid-filled precessing spheroid, which has been well tested numerically and experimentally (see e.g., Noir et al., 2003; Triana et al., 2012). Such misalignment is seen from the mantle frame of reference as a solid body rotation of the fluid core around an *equatorial* axis, and this axis goes around on the equatorial plane with a nearly diurnal frequency (see e.g., Pais & Le Mouël, 2001, for a detailed description of such flow). This motion is in fact another example of a uniform vorticity flow, just like the FCN or the spin-over mode. The core surface flow from precession is about 4.3 mm/s. The corresponding Reynolds number is about $Re \sim 473$, large enough for a fully turbulent boundary flow to develop. Thus, the weaker FCN flow associated with the retrograde annual nutation does not exist in isolation, it

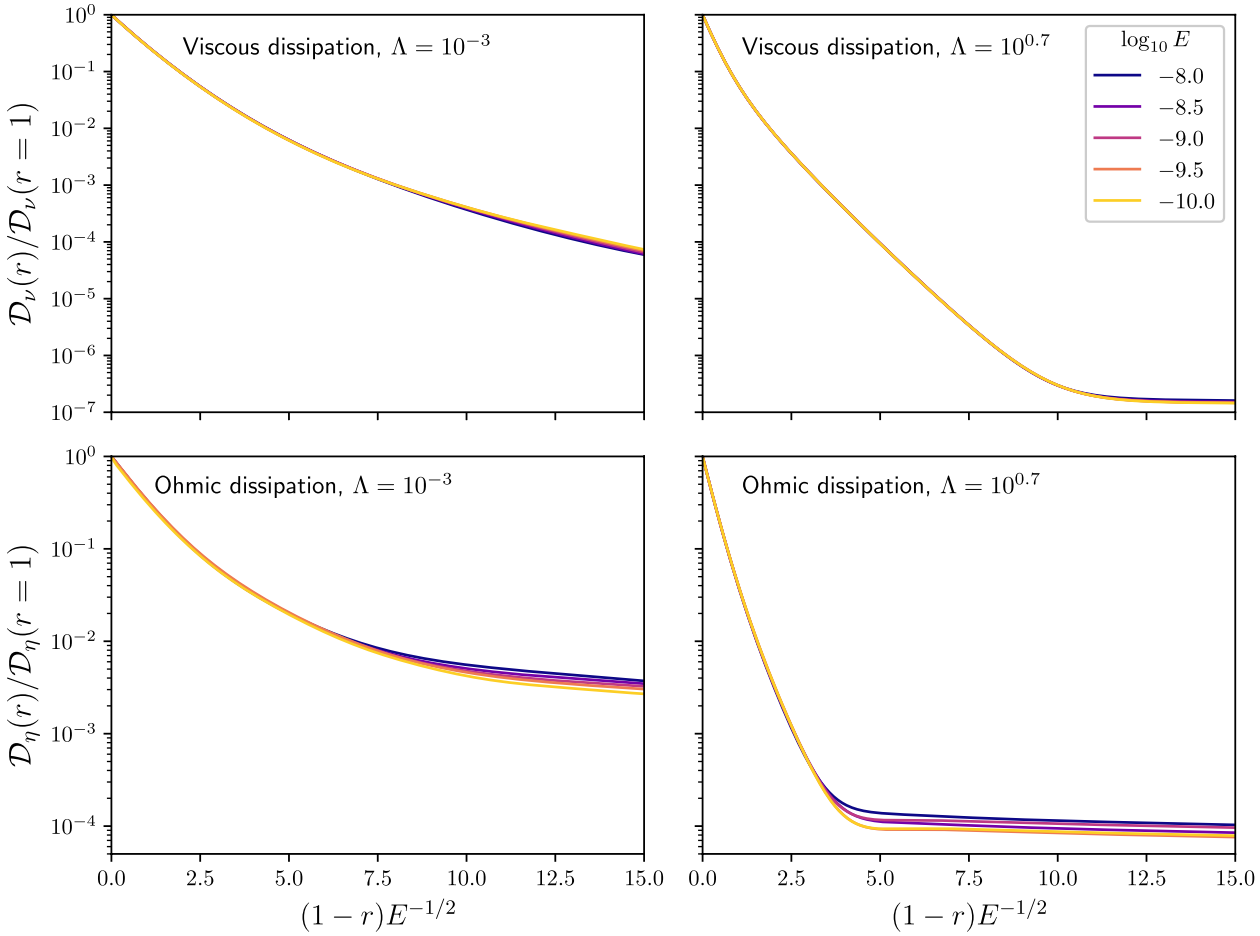

Figure 9. Radial profiles (θ, ϕ integrated) at $P_m = 10^{-3}$ of the viscous (top) and Ohmic dissipation (bottom) near the CMB scaled by their respective maximum values at the CMB. Panels on the left correspond to the hydrodynamic (viscous-dominated) regime at $\Lambda = 10^{-3}$, and panels on the right correspond to $\Lambda \simeq 5.01$ where Ohmic and viscous processes contribute equally to the overall energy dissipation. The horizontal axis is the radial distance to the CMB scaled by $\sqrt{E}$. Colors indicate the Ekman number. Imposed axial uniform field case. CMB, core-mantle boundary.

has a turbulent companion. Nonlinearities will prevent any simple linear superposition of these flows and Reynolds stresses will lead to increased viscous damping of the FCN. Estimating this damping increase remains very challenging, as simple eddy viscosity estimates based on mixing length theory (see e.g., Tennekes & Lumley, 1972) do not seem applicable in this case (Buffett & Christensen, 2007).

The study by Deleplace and Cardin (2006) arrives at an expectation for the value of the effective Ekman number in the core of $E \approx 3 \times 10^{-11}$ to match σ_{obs} when the Elsasser number is set to $\Lambda = 0.145$, with a viscous dissipation 85% of the total. According to our Equation 7, we estimate $E \approx 4 \times 10^{-11}$ if we use the same Λ, the viscous dissipation being 90% of the total (see Figure 5). The slight difference can be traced to our choice of an insulating mantle, whereas in Deleplace and Cardin (2006) there is a thin layer at the bottom of the mantle with the same electrical conductivity as the core, where additional Ohmic dissipation takes place. Mathews and Guo (2005) give an estimate of $E \approx 3.3 \times 10^{-11}$ when $\Lambda \approx 1$ assuming a thin, low conductivity (10 S/m) layer at the bottom of the mantle, which is in fair agreement with our $E = 2.5 \times 10^{-11}$ estimate. Thus, our results largely validate the simpler analytical approach and the approximations made in both Deleplace and Cardin (2006) and Mathews and Guo (2005). The uniform vorticity flow assumption is indeed a good one, at least in the case at hand. Note that unmodelled features such as density stratification at the top of the core, CMB topography, or the back reaction of the mantle on the core might have the potential to change this simple picture dramatically.

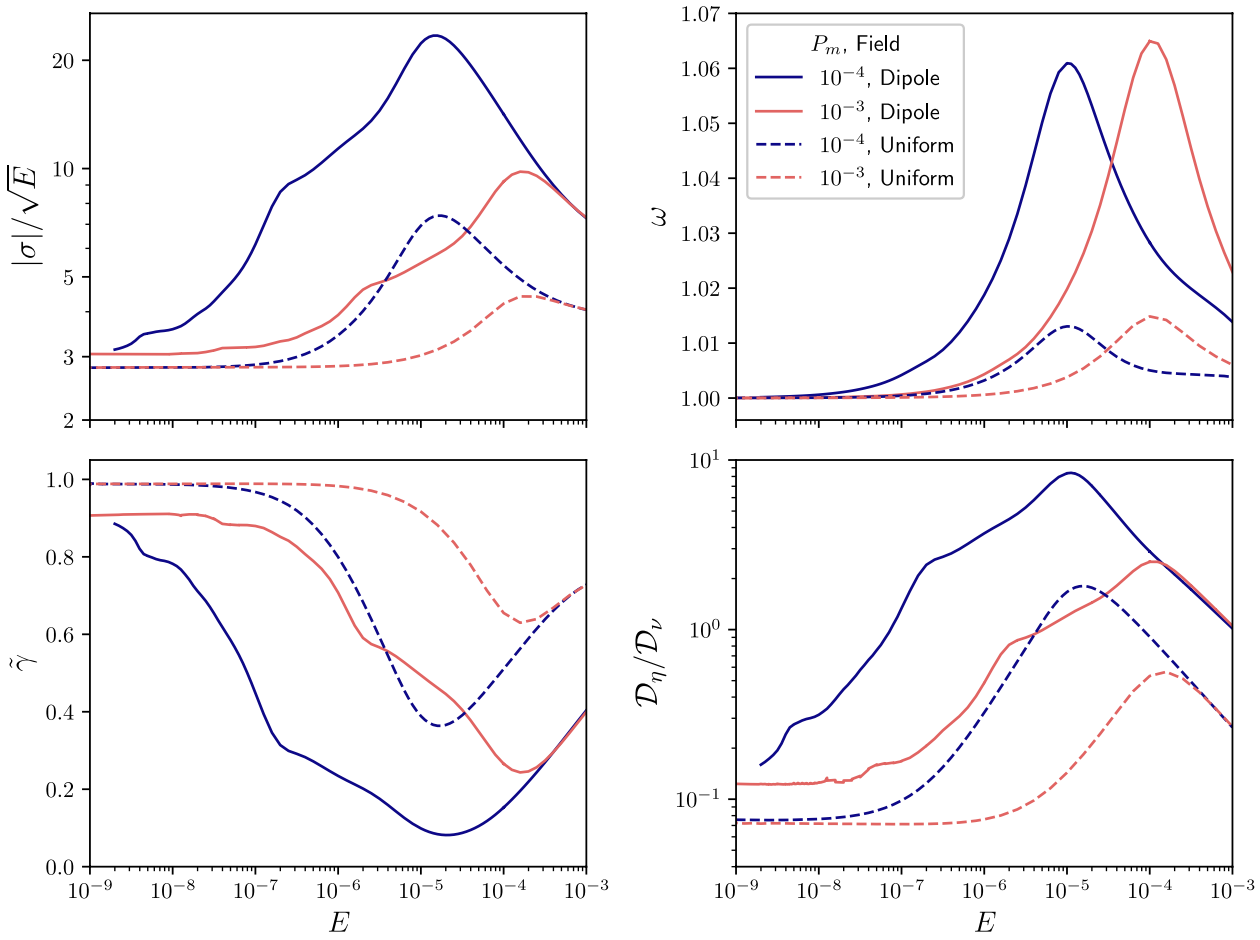

Figure 10. A comparison between the imposed dipolar field (continuous lines) and axial uniform field (dashed lines) over an extended range of E for a fixed Elsasser number $\Lambda = 0.1$. Dark blue lines correspond to $P_m = 10^{-4}$ and red lines to $P_m = 10^{-3}$. Top left panel shows the scaled damping, top right panel shows the mode frequency, bottom left panel shows the ratio $\tilde{\gamma}$ between the magnitude of the CMB torque γ_{cmb} and the quantity $| \sigma | \sqrt{2I}$, see Equation 9. Panel on the bottom right shows the Ohmic to viscous dissipation ratio. CMB, core-mantle boundary.

6. Summary and Conclusions

We have implemented a linear, fully 3D numerical model to study viscous and Ohmic dissipation processes associated with the Earth's FCN mode. Our approach consists of using the spin-over eigenmode as a proxy for the FCN motion, taking advantage of their analogous flow characteristics, and representing the geomagnetic field either as an externally imposed, uniform axial field or as a dipolar field. Deviations from sphericity in the total dissipation are expected to enter only at second order in the ellipticity, as indicated by (Zhang et al., 2004). Thus, by assuming spherical rather than ellipsoidal surfaces at both the ICB and the CMB, we introduce an error smaller than 1% on the total energy dissipation. With spherical surfaces and the aid of an efficient spectral method based on ultraspherical polynomials, we are able to reach very small Ekman numbers ($\sim 10^{-11}$) at an affordable computational cost.

The flow in the model appears to reach an asymptotic regime where the damping scales as $E^{1/2}$ in the numerically accessible Ekman number range. In the case of an imposed axial uniform magnetic field, two asymptotic regimes appear: if the Elsasser number Λ is much smaller than unity, then the dissipation is dominated by viscosity, and the asymptotic regime is essentially the same as in the purely hydrodynamic case. In this situation, the Ohmic to viscous dissipation ratio D_η/D_ν is directly proportional to Λ. When $\Lambda \gtrsim \mathcal{O}(1)$, stronger Ohmic dissipation takes place but never dominates over viscous dissipation processes, both becoming comparable in that range of Λ. The total dissipation scales are still as $E^{1/2}$ in both asymptotic regimes but with a Λ-dependent factor as given by Equation 6 in the latter case. The Ekman boundary layer

in the viscous dominated case ($\Lambda \ll 1$) becomes a slightly thinner Ekman-Hartmann boundary layer when $\Lambda \gtrsim \mathcal{O}(1)$. The magnetic Prandtl number P_m does not seem to play a big role, the damping being nearly independent of it when $P_m \ll 1$.

We also considered an imposed dipolar field to represent the geomagnetic field in the core. In this case, the background magnetic field is stronger near the ICB compared to the field at the CMB (at the same Elsasser number). Although more demanding computationally, we could glimpse asymptotic behavior for a limited range of the control parameters. As in the axial uniform field case, a weak regime also appears for $\Lambda \ll 1$ but it seems dependent on the magnetic Prandtl number P_m. An "intermediate" regime exists when $\Lambda > 3 \times 10^3$ where the P_m dependence weakens. Numerical limitations prevented us from exploring eigensolutions for $\Lambda > 1$. For the dipolar case in general, the ICB contributes more to the damping particularly through more Ohmic heating. However,the total damping comes mostly from Ohmic and viscous dissipation at the CMB.

Our model shows that possible deviations of the core flow from solid body rotation, such as internal shear layers, do not contribute in any significant way to total dissipation. Almost all the kinetic energy is dissipated at the boundaries, mostly at the CMB in both dipolar and uniform background field cases. Taking the Ekman number as a free parameter to match the observed $\mathrm{Im}\{K_{\mathrm{cmb}}\}$, we reach essentially the same estimates as Deleplace and Cardin (2006) and Mathews and Guo (2005), thus validating their much simpler approach. We do see evidence of Ohmic dissipation processes in the bulk of the fluid core that cannot be captured by their models, but they do not appear to take place in the asymptotic regime appropriate for Earth.

There are still many aspects that deserve further study to disentangle the nature of the damping of the Earth's nutations. One of them is the possibility that the boundary layer at the CMB is turbulent, and its effect on the dissipation associated with nutations. Reliable estimates of this dissipation are important since it will tighten the constraints on the conductivity of the Earth's lower mantle, the strength of the magnetic field at the CMB, and possibly the length scale of the CMB topography. Our numerical approach can be readily extended to include mantle conductivity, density stratification, and more complex field geometries. These are topics for future study.

Appendix A: Numerical Method

To formulate the problem as a numerical eigenvalue problem we need a discretization scheme. Both the flow velocity $\boldsymbol{u}$ and the induced magnetic field $\boldsymbol{b}$ are divergenceless, so a poloidal-toroidal representation is adequate:

$$\begin{aligned} \mathbf{u_0} &= \nabla \times \nabla \times \Big[\mathcal{P}(\mathbf{r})\mathbf{r}\Big] + \nabla \times \Big[\mathcal{T}(\mathbf{r})\mathbf{r}\Big], \\ \mathbf{b_0} &= \nabla \times \nabla \times \Big[\mathcal{F}(\mathbf{r})\mathbf{r}\Big] + \nabla \times \Big[\mathcal{G}(\mathbf{r})\mathbf{r}\Big]. \end{aligned} \tag{A1}$$

We use spherical harmonic expansions for the angular dependence of the scalar functions $\mathcal{P}, \mathcal{T}$ and $\mathcal{F}, \mathcal{G}$. We illustrate the method for just one of these scalar functions since it is completely analogous for all of them. For instance, for $\mathcal{F}$ we write

$$\mathcal{F}(r,\theta,\phi) = \sum_{l=1}^{l_{\max}} \sum_{m=-l}^{l} F_{lm}(r) Y_l^m(\theta,\phi), \tag{A2}$$

where Y_l^m are the spherical harmonics, $F_{lm}(r)$ is a radial function, and $l_{\max}$ determines the angular truncation level. The spherical harmonic expansion leads to a fully decoupled problem in the azimuthal wave number m. The FCN has $m = 1$ so we restrict m accordingly. We further expand each function $F_{lm}(r)$ using Chebyshev polynomials t_k:

$$F_{lm}(r) = \sum_{k=0}^{N} F_{lm}^k t_k(r), \tag{A3}$$

where F_{lm}^k is a complex coefficient to be determined, k is the degree of the Chebyshev polynomial, and N is the radial truncation level. We map the natural domain $[-1, 1]$ of the Chebyshev polynomials to the radial interval $[R_{\mathrm{ICB}}, R_{\mathrm{CMB}}] \equiv [0.35, 1]$. For the differential operators appearing in the governing equations

(Section 2.2 in the main text) we employ a fast spectral method devised by Olver and Townsend (2013) that uses Chebyshev polynomials for the unknowns, as just explained, and Gegenbauer polynomials for terms involving their spatial derivatives. In the end, we have transformed our original problem into a generalized eigenvalue problem of the form

$$\mathbf{A}\mathbf{x} = \lambda\mathbf{B}\mathbf{x}, \tag{A4}$$

where $\mathbf{A}$ and $\mathbf{B}$ are sparse matrices, λ is the eigenvalue, and $\mathbf{x}$ is the eigenvector comprised by the set of coefficients $\{P_{lm}^k, T_{lm}^k, F_{lm}^k, G_{lm}^k\}$.

We employ no-slip ($\boldsymbol{u} = 0$) boundary conditions for the velocity, therefore, we set

$$\begin{aligned} P_{lm}(r_b) = P'_{lm}(r)\Big|_{r=r_b} &= 0, \\ T_{lm}(r_b) &= 0, \end{aligned} \tag{A5}$$

where r_b denotes the radius of either the ICB and the CMB, and the prime ($'$) denotes a radial derivative. For the induced magnetic field $\boldsymbol{b}$ we assume an insulating mantle and insulating inner core, thus in these regions $\boldsymbol{b}$ can be written as a potential field $\boldsymbol{b} = \nabla\,\Phi$. This condition is met if the radial functions satisfy

$$\begin{aligned} l\frac{F_{lm}(r_{\rm icb})}{r_{\rm icb}} - F'_{lm}(r)\Big|_{r=r_{\rm icb}} &= 0, \\ G_{lm}(r_{\rm icb}) &= 0, \end{aligned} \tag{A6}$$

at the ICB, and

$$\begin{aligned} (l+1)\frac{F_{lm}(r_{\rm cmb})}{r_{\rm cmb}} + F'_{lm}(r)\Big|_{r=r_{\rm cmb}} &= 0, \\ G_{lm}(r_{\rm cmb}) &= 0, \end{aligned} \tag{A7}$$

at the CMB.

The solutions for $\boldsymbol{u}$ are either equatorially symmetric or antisymmetric. Since our applied field $B_0\hat{\mathbf{z}}$ is equatorially antisymmetric, we expect the induced magnetic field $\boldsymbol{b}$ to have the opposite symmetry of $\boldsymbol{u}$. Note also that we do not need to compute all the coefficients for each l since either even or odd l coefficients will vanish depending on the symmetry of $\boldsymbol{u}$ or $\mathbf{b}$. To solve Equation A4 we employ the *shift-and-invert* strategy with the help of the PETSc and SLEPc solver packages and associated libraries (Amestoy et al., 2001, 2006; Balay et al., 1997; Dalcin et al., 2011; Hernandez et al., 2005; Li & Demmel, 2003).

Once we obtain the solutions, we proceed to compute their Ohmic and viscous dissipation. We define first the *radial* Q_{lm} and *consoidal* S_{lm} functions as

$$\begin{aligned} Q_{lm}(r) &= l(l+1)P_{lm}(r), \\ S_{lm}(r) &= P'_{lm}(r) + \frac{P_{lm}(r)}{r}. \end{aligned} \tag{A8}$$

For the sake of compactness we now define

$$q \equiv Q_{lm}(r), \quad s \equiv S_{lm}(r), \quad t \equiv T_{lm}(r). \tag{A9}$$

With this notation, and employing the Schmidt semi-normalized Spherical Harmonic convention, we write the total Ohmic dissipation as

$$\begin{aligned} \mathcal{D}_\eta &= \frac{1}{2}\int_V \left|\nabla\times\mathbf{b}\right|^2 \mathrm{d}V \\ &= Le^2 E_\eta \sum_{l=m}^{l_{\max}} \frac{4\pi}{2l+1}\int_{r_{\rm icb}}^{r_{\rm cmb}} l(l+1)\left[l(l+1)\left|t\right|^2 + \left|t + rt'\right|^2 + \left|q - s - rs'\right|^2\right]\mathrm{d}r, \end{aligned} \tag{A10}$$

where V is the fluid domain. Similarly, we compute the viscous energy dissipation as

$$\begin{aligned}\mathcal{D}_\nu &= E\int_V \widehat{\nabla\mathbf{u}} : \widehat{\nabla\mathbf{u}}\,\mathrm{d}V \\ &= E\sum_{l=m}^{l_{\max}} \frac{4\pi}{2l+1}\int_{r_{\mathrm{icb}}}^{r_{\mathrm{cmb}}} \Big\{3\left|rq'\right|^2 + l(l+1)\Big(\left|rt'-t\right|^2 + \left|q+rs'-s\right|^2\Big) \\ &\quad + l(l-1)(l+1)(l+2)\Big(\left|s\right|^2 + \left|t\right|^2\Big)\Big\}\mathrm{d}r,\end{aligned} \tag{A11}$$

where the colon (:) denotes the tensor double dot product and $\widehat{\nabla\mathbf{u}}$ is defined as

$$\widehat{\nabla\mathbf{u}} = \frac{1}{2}\Big[\nabla\mathbf{u} + \left(\nabla\mathbf{u}\right)^T\Big], \tag{A12}$$

All the formulae in this study were obtained with the help of TenGSHui, a tensor calculus package for Mathematica (Trinh, 2019). The computation of the matrix elements involve the usage of the Wigner-3j symbols, which we compute with the help of the package WIGXJPF (Johansson & Forssén, 2016).

Appendix B: The Damping of the Spin-Over Mode in an Oblate Spheroid

The effect of a small amount of viscous dissipation on the inertial eigenmodes, including the spin-over mode, of an axisymmetric spheroid has been computed by Zhang et al. (2004). The damping factor σ of the spin-over mode and its frequency ω are given by:

$$\begin{aligned}\sigma &= E^{1/2}\Big[2.62047 + 0.42634\epsilon^2 + \mathcal{O}(\epsilon^4)\Big], \\ \omega &= \frac{2}{2-\epsilon^2} + E^{1/2}\Big[0.25846 + 0.76633\epsilon^2 + \mathcal{O}(\epsilon^4)\Big],\end{aligned} \tag{B1}$$

where ϵ is the eccentricity of the bounding spheroid and E is the Ekman number. With no-slip boundary conditions as assumed here, most of the kinetic energy is dissipated within the boundary layer. The damping factor σ in Equation B1 depends only to second order in the eccentricity ϵ. Given that $\epsilon^2 \sim 0.007$ for the Earth's CMB, a spherical approximation would introduce a relative error on the energy dissipation smaller than 1%.

Data Availability Statement

The code implementing the model described in this study is freely available at https://bitbucket.org/repepo/kore/src/master. All the scripts and associated data necessary to reproduce all the figures in this paper are archived along with the code.

Acknowledgments
The authors would like to thank Bruce Buffett, Mathieu Dumberry, and an anonymous reviewer for their insightful and constructive comments. The authors wish to express our gratitude also to Tim Van Holst and Ankit Barik for their comments on early versions of this study. The research leading to these results has received funding from the European Research Council (ERC) under the European Union's Horizon 2020 research and innovation program (Advanced Grant agreement no. 670874, ROTANUT, and Synergy Grant agreement no. 855677 GRACEFUL).

References

Amestoy, P. R., Duff, I. S., L'Excellent, J.-Y., & Koster, J. (2001). A fully asynchronous multifrontal solver using distributed dynamic scheduling. *SIAM Journal on Matrix Analysis and Applications*, *23*(1), 15–41. https://doi.org/10.1137/s0895479899358194

Amestoy, P. R., Guermouche, A., L'Excellent, J.-Y., & Pralet, S. (2006). Hybrid scheduling for the parallel solution of linear systems. *Parallel Computing*, *32*(2), 136–156. https://doi.org/10.1016/j.parco.2005.07.004

Balay, S., Gropp, W. D., McInnes, L. C., & Smith, B. F. (1997). Efficient management of parallelism in object oriented numerical software libraries. In E. Arge, A. M. Bruaset, & H. P. Langtangen (Eds.), Eds., *Modern software tools in scientific computing* (pp. 163–202). Birkhäuser Press.

Benton, E. R., & Loper, D. E. (1969). On the spin-up of an electrically conducting fluid. Part 1: The unsteady hydromagnetic ekman-hartmann boundary-layer problem. *Journal of Fluid Mechanics*, *39*(3), 561–586. https://doi.org/10.1017/s0022112069002333

Buffett, B., Mathews, P., & Herring, T. (2002). Modeling of nutation and precession: Effects of electromagnetic coupling. *Journal of Geophysical Research: Solid Earth*, *107*(B4), ETG–5. https://doi.org/10.1029/2000jb000056

Buffett, B. A. (1992). Constraints on magnetic energy and mantle conductivity from the forced nutations of the earth. *Journal of Geophysical Research*, *97*(B13), 19581–19597. https://doi.org/10.1029/92jb00977

Buffett, B. A. (2010). Tidal dissipation and the strength of the Earth's internal magnetic field. *Nature*, *468*(7326), 952. https://doi.org/10.1038/nature09643

Buffett, B. A., & Christensen, U. R. (2007). Magnetic and viscous coupling at the core-mantle boundary: Inferences from observations of the Earth's nutations. *Geophysical Journal International*, *171*(1), 145–152. https://doi.org/10.1111/j.1365-246x.2007.03543.x

Busse, F. H. (1968). Steady fluid flow in a precessing spheroidal shell. *Journal of Fluid Mechanics*, *33*(4), 739–751. https://doi.org/10.1017/s0022112068001655

Cébron, D., Laguerre, R., Noir, J., & Schaeffer, N. (2019). Precessing spherical shells: Flows, dissipation, dynamo and the lunar core. *Geophysical Journal International*, *219*(Supplement_1), S34–S57. https://doi.org/10.1093/gji/ggz037

Christensen, U. R., & Aubert, J. (2006). Scaling properties of convection-driven dynamos in rotating spherical shells and application to planetary magnetic fields. *Geophysical Journal International*, *166*(1), 97–114. https://doi.org/10.1111/j.1365-246x.2006.03009.x

Dalcin, L. D., Paz, R. R., Kler, P. A., & Cosimo, A. (2011). Parallel distributed computing using Python. *Advances in Water Resources*, *34*(9), 1124–1139. https://doi.org/10.1016/j.advwatres.2011.04.013

Deleplace, B., & Cardin, P. (2006). Viscomagnetic torque at the core mantle boundary. *Geophysical Journal International*, *167*(2), 557–566. https://doi.org/10.1111/j.1365-246x.2006.03180.x

Gans, R. F. (1972). Viscosity of the Earth's core. *Journal of Geophysical Research*, *77*(2), 360–366. https://doi.org/10.1029/jb077i002p00360

Greenspan, H. (1968). *The theory of rotating fluids*. Cambridge University Press.

Hernandez, V., Roman, J. E., & Vidal, V. (2005). SLEPc: A scalable and flexible toolkit for the solution of eigenvalue problems. *ACM Transactions on Mathematical Software*, *31*(3), 351–362. https://doi.org/10.1145/1089014.1089019

Johansson, H. T., & Forssén, C. (2016). Fast and accurate evaluation of Wigner 3j, 6j, and 9j symbols using prime factorization and multiword integer arithmetic. *SIAM Journal on Scientific Computing*, *38*(1), A376–A384. https://doi.org/10.1137/15M1021908

Koot, L., & Dumberry, M. (2013). The role of the magnetic field morphology on the electromagnetic coupling for nutations. *Geophysical Journal International*, *195*(1), 200–210. https://doi.org/10.1093/gji/ggt239

Koot, L., Dumberry, M., Rivoldini, A., De Viron, O., & Dehant, V. (2010). Constraints on the coupling at the core-mantle and inner core boundaries inferred from nutation observations. *Geophysical Journal International*, *182*(3), 1279–1294. https://doi.org/10.1111/j.1365-246x.2010.04711.x

Le Bars, M., Cébron, D., & Le Gal, P. (2015). Flows driven by libration, precession, and tides. *Annual Review of Fluid Mechanics*, *47*, 163–193. https://doi.org/10.1146/annurev-fluid-010814-014556

Li, X. S., & Demmel, J. W. (2003). SuperLU: A scalable distributed-memory sparse direct solver for unsymmetric linear systems. *ACM Transactions on Mathematical Software*, *29*(2), 110–140. https://doi.org/10.1145/779359.779361

Lin, Y., & Ogilvie, G. I. (2018). Tidal dissipation in rotating fluid bodies: The presence of a magnetic field. *Monthly Notices of the Royal Astronomical Society*, *474*(2), 1644–1656. https://doi.org/10.1093/mnras/stx2764

Lorenzani, S., & Tilgner, A. (2001). Fluid instabilities in precessing spheroidal cavities. *Journal of Fluid Mechanics*, *447*, 111. https://doi.org/10.1017/s002211200100581x

Mathews, P. M., & Guo, J. Y. (2005). Viscoelectromagnetic coupling in precession-nutation theory. *Journal of Geophysical Research: Solid Earth*, *110*(B2). https://doi.org/10.1029/2003jb002915

Mathews, P. M., Herring, T. A., & Buffett, B. A. (2002). Modeling of nutation and precession: New nutation series for nonrigid earth and insights into the earth's interior. *Journal of Geophysical Research: Solid Earth*, *107*(B4). ETG–3. https://doi.org/10.1029/2001jb000390

Moffatt, K., & Dormy, E. (2019). *Self-exciting fluid dynamos*. Cambridge, UK: Cambridge University Press.

Noir, J., Cardin, P., Jault, D., & Masson, J.-P. (2003). Experimental evidence of non-linear resonance effects between retrograde precession and the tilt-over mode within a spheroid. *Geophysical Journal International*, *154*(2), 407–416. https://doi.org/10.1046/j.1365-246x.2003.01934.x

Olver, S., & Townsend, A. (2013). A fast and well-conditioned spectral method. *SIAM Review*, *55*(3), 462–489. https://doi.org/10.1137/120865458

Pais, M. A., & Le Mouël, J. L. (2001). Precession-induced flows in liquid-filled containers and in the Earth's core. *Geophysical Journal International*, *144*(3), 539–554. https://doi.org/10.1046/j.1365-246x.2001.01367.x

Palmer, A., & Smylie, D. (2005). VLBI observations of free core nutations and viscosity at the top of the core. *Physics of the Earth and Planetary Interiors*, *148*(2–4), 285–301. https://doi.org/10.1016/j.pepi.2004.09.003

Rekier, J., Triana, S. A., Trinh, A., & Dehant, V. (2020). Inertial modes of a freely rotating ellipsoidal planet and their relation to nutations. *The Planetary Science Journal*, *1*(1), 20.

Rekier, J., Trinh, A., Triana, S. A., & Dehant, V. (2019). Internal energy dissipation in Enceladus's subsurface ocean from tides and libration and the role of inertial waves. *Journal of Geophysical Research: Planets*, *124*(8), 2198–2212. https://doi.org/10.1029/2019je005988

Rieutord, M., Georgeot, B., & Valdettaro, L. (2001). Inertial waves in a rotating spherical shell: Attractors and asymptotic spectrum. *Journal of Fluid Mechanics*, *435*, 103–144. https://doi.org/10.1017/s0022112001003718

Rogister, Y., & Valette, B. (2009). Influence of liquid core dynamics on rotational modes. *Geophysical Journal International*, *176*(2), 368–388. https://doi.org/10.1111/j.1365-246x.2008.03996.x

Schmitt, D. (2006). Numerical study of viscous modes in a rotating spheroid. *Journal of Fluid Mechanics*, *567*, 399–414. https://doi.org/10.1017/s0022112006002497

Schmitt, D. (2012). Quasi-free-decay magnetic modes in planetary cores. *Geophysical & Astrophysical Fluid Dynamics*, *106*(6), 660–680. https://doi.org/10.1080/03091929.2012.681306

Sous, D., Sommeria, J., & Boyer, D. (2013). Friction law and turbulent properties in a laboratory Ekman boundary layer. *Physics of Fluids*, *25*(4), 046602. https://doi.org/10.1063/1.4802045

Tennekes, H., & Lumley, J. L. (1972). *A first course in turbulence*. The MIT Press.

Tilgner, A. (2007). 8.07 - rotational dynamics of the core. In G. Schubert (Ed.), Ed., *Treatise on geophysics* (pp. 207–243). Elsevier.

Triana, S. A., Rekier, J., Trinh, A., & Dehant, V. (2019). The coupling between inertial and rotational eigenmodes in planets with liquid cores. *Geophysical Journal International*, *218*(2), 1071–1086. https://doi.org/10.1093/gji/ggz212

Triana, S. A., Zimmerman, D., & Lathrop, D. (2012). Precessional states in a laboratory model of the earth's core. *Journal of Geophysical Research: Solid Earth*, *117*(B4). https://doi.org/10.1029/2011jb009014

Trinh, A. (2019). *Modeling the interior of Enceladus: A combined view from gravity, topography, and libration (Unpublished doctoral dissertation)*. Université Catholique de Louvain.

Zhang, K., Liao, X., & Earnshaw, P. (2004). On inertial waves and oscillations in a rapidly rotating spheroid. *Journal of Fluid Mechanics*, *504*, 1–40. https://doi.org/10.1017/s0022112003007456